

Article

Examining Energy Storage Potential in Weakly Polar Nematic Liquid Crystals Infused with Anthraquinone Dye: A Comprehensive Approach

Bhupendra Pratap Singh ^{1,2} , Shikha Agarwal ² , Mohammad Rafe Hatshan ³ , Keshav Kumar Singh ⁴,
Kulurumotlakatla Dasha Kumar ⁵, Rajiv Manohar ², Pankaj Kumar Tripathi ^{6,*} 
and Dharmendra Pratap Singh ^{7,*} 

- ¹ Department of Electro-Optical Engineering, National United University, No. 2, Lien-Da, Miaoli 360, Taiwan; bhupendraphy@gmail.com
 - ² Liquid Crystal Research Lab, Department of Physics, University of Lucknow, Lucknow 226007, Uttar Pradesh, India; agashikha1995@gmail.com (S.A.); rajiv.manohar@gmail.com (R.M.)
 - ³ Department of Chemistry, College of Science, King Saud University, Riyadh 11451, Saudi Arabia; mhatshan@ksu.edu.sa
 - ⁴ Department of Physics, University of Lucknow, Lucknow 226007, Uttar Pradesh, India; keshavsinghi007@gmail.com
 - ⁵ Graduate School of Convergence Science, Department of Applied Hybrid Materials, Pusan National University, San 30 Jangjeon-dong, Geumjeong-gu, Busan 609-735, Republic of Korea; dashakumar1212@gmail.com
 - ⁶ Department of Physics, Sharda University, Knowledge Park III, Greater Noida 201310, Uttar Pradesh, India
 - ⁷ Unité de Dynamique et Structure des Matériaux, Moléculaires (UDSMM), Université du Littoral Côte d'Opale (ULCO), 50 Rue Ferdinand Buisson, 62228 Calais, France
- * Correspondence: pankajtripathi19@gmail.com (P.K.T.); dharmendra.singh@univ-littoral.fr (D.P.S.); Tel.: +33-(0)3-21-46-57-58 (D.P.S.)

Abstract: The applications of liquid crystals in the field of renewable, clean and sustainable technologies of energy storage are of utmost importance at present. This paper delves into dielectric spectroscopic studies of a weakly polar nematic liquid crystal (NLC) enriched with an anthraquinone dye. The primary objective is to assess the impact of increasing dye concentrations on various properties. Anthraquinone dye has been found to increase the dielectric permittivity of weakly polar NLC, leading to a 4.7-fold increase in dielectric anisotropy. Simultaneously, a reduction of around 11% in threshold and operating voltages of the NLC has also been recorded after using dye as the guest material. The added dipolar contributions provided by dye molecules have been attributed to this surplus permittivity. The NLC has been found to have an approximately 54% faster response to the applied field. The intrinsic polarization field of dye molecules accelerates nearby LC molecule reorientation, leading to a 56.5% faster fall time and a 29.8% faster rise time in a 3.0 wt% dye-doped LC cell. These experimental results have been validated via computational studies as well. The simulation results about dipole moment and polarizability provide robust support for our experimental results. Such composites evince their potential for energy storage and 5G communication technologies with adjustable impedance and permittivity.

Keywords: liquid crystal; response time; capacitance; dielectric properties; tunability; density functional theory; dye-doped liquid crystal; energy storage; tunable material; anthraquinone dyes; computational studies



Citation: Singh, B.P.; Agarwal, S.; Hatshan, M.R.; Singh, K.K.; Kumar, K.D.; Manohar, R.; Tripathi, P.K.; Singh, D.P. Examining Energy Storage Potential in Weakly Polar Nematic Liquid Crystals Infused with Anthraquinone Dye: A Comprehensive Approach. *J. Compos. Sci.* **2023**, *7*, 470. <https://doi.org/10.3390/jcs7110470>

Received: 18 September 2023

Revised: 29 October 2023

Accepted: 7 November 2023

Published: 10 November 2023



Copyright: © 2023 by the authors. Licensee MDPI, Basel, Switzerland. This article is an open access article distributed under the terms and conditions of the Creative Commons Attribution (CC BY) license (<https://creativecommons.org/licenses/by/4.0/>).

1. Introduction

The very first published finding of dye orientation in a nematic host sparked widespread interest in using dye molecules in liquid crystal devices, and innumerable modes of guest-host-based device operation have since been proposed [1–3]. These devices work on the concept that the guest chromophore aligns with the liquid crystal (LC) host, changing the

orientation of the matrix from an absorbing (colored) state to a transmitting (colorless) one by applying an electric field. This is due to the dye's absorption transition being oriented along a certain axis. The alignment of dye within the LC medium is of ultimate relevance for the visible characteristics of a system since it is determined by the color and absorption coefficient of the dye, its solubility in the host and the contrast ratio between the absorbing and transmitting states. To give an acceptable operation lifespan to a device, the system must also be stable concerning external factors such as heat, light and electricity. Consequently, selecting the right dye and an appropriate host liquid crystal, in addition to ensuring that they work well together, is essential for designing an effective device. Azo dyes were initially proposed for usage in LC-based guest-host applications because of their elongated, rod-shaped molecules and dichroic behavior which aids in better alignment with an LC host composed of rod-like molecules [4]. Even though azo dye's well-established synthetic chemistry facilitates a wide range of colors, the restricted photochemical and electrochemical stabilization could be an obstruction to their utilization in commercial devices [5].

Anthraquinone dye has been recommended as an alternative option as guests in a host LC matrix since it is more stable than azo dye. Anthraquinones are tricyclic organic molecules with unique fluorescent characteristics and exhibit higher resistance to photo-bleaching [6]. Nevertheless, generally, its molecular form is often less rod-like, resulting in a comparatively disordered alignment in a constraint medium such as a liquid crystalline one [7]. Although it has been shown that many anthraquinone dyes align well inside the liquid crystal hosts, their typically lower dichroic ratios in comparison to azo dyes [8,9] limit their useful applications. According to several theories, this effect is caused by an inadequate alignment of the electronic transition dipole moment (TDM) with the anthraquinone dye's long molecular axis, which results in changing the substantial angle (β) [10]. Notably, some anthraquinone dyes have superior alignment within liquid crystal (LC) hosts; however, acquiring a broad spectrum of colors with higher adsorption coefficients, on the other hand, has proven to be challenging [8,11]. Moreover, the reported literature depicts a number of anthraquinone dyes that have been prepared and tested for guest-host applications. A variety of colors can be produced by altering the position and type of the substituents. Numerous different dyes including tetrazine [12], naphthalene [13], perylene [14] and acenequinone [15] have been synthesized for prospective use in guest-host applications, demonstrating the broad spectrum of compounds that are potential candidates for these applications. To build a suitable guest-host liquid crystal device, multiple design parameters referring to several interlinked characteristics must be met simultaneously. The overall goal is to address the design of liquid crystal hosts and dyes individually; however, the major drawback is the complexity of dyes meeting the stringent standards. Prior investigation has shown that anthraquinone dye is a promising candidate for guest-host-based LC devices.

To be used successfully in real-world display and non-display technologies it is preferable to use a framework based on the logical design of both guest-host material, taking into account the many conditions that guest-host systems must satisfy. To support a strategy for the possible applications, a scientific knowledge of the characteristics that describe the behavior is a necessary prerequisite. In these applications, the host system also plays a crucial role. Therefore, the dispersion of dyes in different mesophases such as nematic [16–18], cholesteric [19,20], ferroelectric [21,22] and smectic [23–25] systems have already been tested for different application purposes. Nematic systems are the most fundamental and thoroughly investigated out of all other host mesophases. Additionally, it is reported that the chiral nematic phase can enhance optical efficiency, whereas the smectic A (SmA) phase may offer superior bi-stability [26,27], providing the possibility of devices with a lower power consumption as compared to other guest-host based devices. However, their primary application in display devices has received the most attention. Nevertheless, the dyes in liquid crystal hosts have been proposed as the building blocks for a wide range of non-display applications including, advanced textiles [28,29], augmented reality (AR)

and virtual reality (VR) systems [30,31], optical shutters [32,33], biosensing [34,35], liquid crystal lasers [36], liquid crystal lenses [37,38], soft actuators [39,40], smart windows [41,42] and optical storage devices [43,44].

Research and development in the arena of advancement towards clean and sustainable strategies for energy storage, such as batteries, supercapacitors, fuel cells, etc., has been receiving overwhelming interest in recent years towards storing energy in a sustainable way [45–49]. A great potential in the empowerment of portable electronics has been exhibited by electrochemical energy storage systems. The main components of any energy storage device consist of electrodes and electrolytes to provide a suitable transportation of ions through anode to cathode during the process of charge storage and its eventual discharging. Ionic liquids (ILs) possessing fair ionic conductivity, thermal stability and electrochemical stability deliver good performance when used as the prime component of energy storage devices. Compared to ILs, ionic liquid crystals (ILCs) bestowed with synergistic properties of both liquid crystals and ionic liquids are nowadays given much greater importance in flexible electronics to prove its efficient candidature for advanced functional applications such as stimuli-responsive conductors for energy storage devices, flexible batteries, etc. [50–52]. Liquid crystals are promising functional materials to be used in a variety of different renewable technologies as they are capable of interacting with external stimuli such as electric and magnetic fields, incident light or different frequencies, etc., and responding to them. These external stimuli are capable of tailoring the anisotropic properties of liquid crystals. Furthermore, the addition of nanostructures and organic dopants tend to enrich the features of liquid crystals for device applications. Various researchers have found different mesophases and different guest–host composites systems suitable for such applications [53–57]. The inclusion of dye in even a trace amount enhances the electrical properties of LCs considerably and thereby improves the performance of the concerned devices. Wu. et al. found that ionic impurities can be easily suppressed by adding methyl red dye in LCs, which leads to a better voltage holding ratio in the system [58]. Different reports are available that show the dispersion of different dyes leads to improved electro-optical and mechanical properties of LCs and reduces the operating voltage considerably [59–62]. The interdependency of electro-optical characteristics of azo-dye and anthraquinone dyes in polymer-dispersed liquid crystals (PDLCs) has been studied by P. Kumar et al. They found that at lower dye concentrations, anthraquinone tends to offer a better contrast ratio as compared to the azo-dyed-LC systems [63]. Recently, a report has been published by S. Agarwal et al. about a tunable optical filter based on the attributes of dye-dispersed nematic liquid crystal. The photoisomerization induced in the dye in the constraint medium was attributed to the device performance. The functional material also displayed notable energy and charge storage capability [64]. Henceforth, it can be seen that different dyes have been explored in liquid crystalline matrix for a variety of applications. However, the effect of anthraquinone dye on weakly polar nematic liquid crystals (NLCs) is yet to be extensively investigated.

This study endeavors to investigate the interaction between anthraquinone dye and weakly polar liquid crystal (LC) molecules, elucidate their integration within the structural framework of weakly polar LCs, and explore their influence on the physical, dielectric and electro-optical characteristics of the host nematic LCs. The research employs voltage-dependent transmittance measurements to examine the threshold and driving voltages of both pure LC systems and LCs dispersed with the dye. Additionally, dielectric spectroscopy is employed to ascertain the dielectric anisotropy of the LC material. To gain insights into the response of anthraquinone dye-doped LC systems to an applied field, the response time of LC cells containing the dye is assessed. Furthermore, the study delves into the potential utility of the ideal LC–dye combination for applications such as energy harvesting and other technological uses. In conjunction with experimental investigations, computational studies are also conducted in the isolated gas phase, focusing on LC and dye molecules. These computational simulations aim to provide a deeper understanding of the geometric alterations that transpire within the LC when doped with the appropriate dye. Additionally,

they seek to unravel the molecular-level interactions between the guest dye molecules and the host LC molecules.

2. Materials and Methods

2.1. Details of the Host and Guest Materials

As the host material, a weakly polar nematic LC 4,4'-di-pentyl-azoxy-benzene (D5AOB) LC (Frinton Laboratories, Hainesport, NJ, USA) was used. The D5AOB LC exhibits positive dielectric anisotropy ($\Delta\epsilon = +0.30$) and the phase sequence is as follows.

Crystal \rightleftharpoons 22°C \rightleftharpoons Nematic (N) \rightleftharpoons 65°C \rightleftharpoons Isotropic

The molecular structure of D5AOB mesophase is shown in Figure 1a. The 4,4'-di-alkyl-azoxy-benzenes (DnAOB) are roughly symmetric and have a nonpolar configuration. In the structure of D5AOB, the long molecular axis deviates from the field direction, offering an advantage in the structure of D5AOB. The dipole moment of the host nematic LC is 1.70 D, and the angle between the dipole and the long molecule axis is 64.9° [65]. We present investigations on the mentioned host NLC doped with an anthraquinone dye (guest); a 2,6-disubstituted anthraquinone dye (26B3OH) synthesized by using a technique reported by Goodby et al. [66], the molecular structure of the dye being depicted in Figure 1b, which is particularly interesting as an LC guest dye due to its relatively rod-like molecular shape which helps it in achieving better molecular alignment in the nematic LC host (a concept of anisotropy matching). Also, the electronic transition dipole moment (TDM) vector of 26B3OH dye becomes highly aligned with the director of nematic LC [67], as shown in Figure 2.

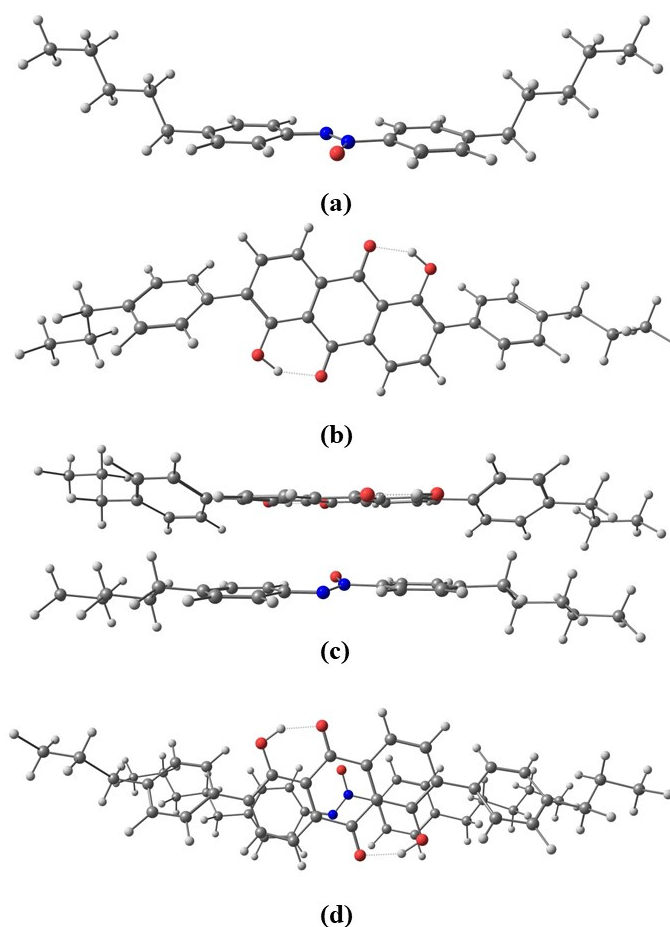


Figure 1. Optimized structure of (a) D5AOB nematic LC, (b) 26B3OH dye, (c) LC–dye complex side view and (d) LC–dye complex top view. All structures are calculated at APFD/6-311++G(d,p) level of theory.

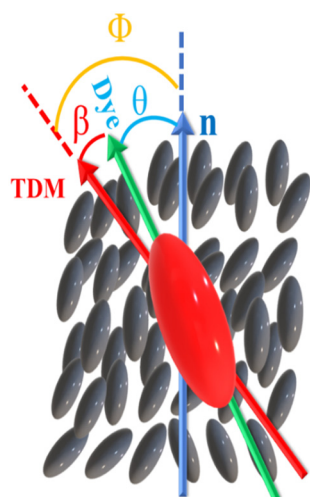


Figure 2. The schematic illustration of a dye molecule (green) inside a host nematic liquid crystal (blue). The director, n , provides the average orientation of the host molecules, and the relative orientations of the dye's long molecular axis (green) and its TDM (red) are given with the specified angles.

2.2. Experimental Techniques

To design the optimum characteristics for dyes in weakly polar liquid crystal hosts, we present a novel computational method that combines density functional theory (DFT) calculations with experimental data from the system under consideration. For the measurement of dielectric properties, the indium-tin-oxide (ITO)-coated glass substrates have been used for the preparation of sample holders having parallel-plate capacitor-type configuration. Horizontal alignment polyimide has been coated on the inner side of these substrates for providing planar alignment to the LC molecules. The detailed procedure for preparing such sample holder is described in our earlier published articles [68,69]. The thickness of these sample holders was confirmed to be $\sim 5.2 \pm 0.05 \mu\text{m}$ using optical interferometry.

LC–dye mixtures were prepared with concentrations of dye fixed to 0.5, 1.0, 1.5, 2.0 and 3.0 wt%. An adequate amount of dye was mixed into a fixed quantity of the host LC, and the mixtures were vigorously stirred at temperature above isotropic point of LC. No solvent has been used for dispersing dye into the LC. Conventional capillary action has been employed for filling the composites in the sample holders meticulously. The highest possible concentration of dye that was uniformly dispersed into the LC was observed to be 3.0 wt% due to challenges in achieving effective mixing at higher concentrations, which resulted in the dye settling at the bottom of the container.

The measurement of dielectric properties as a function of frequency and voltage has been performed by employing a computer-controlled impedance/Gain phase analyzer (HP4194A) for a frequency range from 100 Hz to 10 MHz at an applied alternating field of $0.01 \text{ V}/\mu\text{m}$. The storage component (real part) ϵ' and the loss component (imaginary part) ϵ'' of complex dielectric permittivities along with dielectric anisotropy were obtained. To yield voltage-dependent dielectric parameters, a fixed dc bias of 20 V was applied on the samples.

The voltage-dependent transmittance (VT Curve) and electro-optical dynamic response time for the pure and dye-dispersed D5AOB were recorded in the following manner: Sample holder was placed between crossed polarizers such that the director made an angle of 45° with the transmission axis of each of the polarizers. This system was irradiated with He-Ne laser light of power 10 mW (wavelength 632.8 nm) after providing adequate attenuation by the neutral density (ND) filter. A square wave input signal of frequency 1 kHz was applied on the sample cell and the transmission spectra was recorded as a function of input voltage with the aid of photodiode with a detection time of 100 μs . Furthermore, an amplitude modulated signal with carrier frequency 1 kHz and amplitude 20 V modulated by a square wave of frequency 50 mHz was applied to the same sample holder

to test the electro-optical dynamic response. Signal generator (Agilent 33220A) was used to feed this signal at the inputs of the sample holder and the data were recorded on a digital oscilloscope (Tektronix TDS 2024C) and averaged 32 times to filter out background noise.

2.3. Density Functional Theory (DFT) Simulation

Density functional simulations were performed to investigate the structure and linear and nonlinear optical properties of the liquid crystal D5AOB, 26B3OH anthraquinone dye and their complex. Since the structure of D5AOB is already known, its input structure was taken from the PubChem repository (CID: 10736623). The structure of 26B3OH dye was built by using *Gauss view 5.0* software [70]. These structures represent gas phase D5AOB and 26B3OH dye molecules. To study the interactions and possible structure between two molecules, a gas phase simulation is sufficient. As such, we optimized both structures to minimum energy at the wB97XD/6-311++G(d,p) and APFD/6-311++G(d,p) levels of theory using the *Gaussian 16 program package* [71]. The functional wB97XD is a range-separated function known accurately to predict energies especially when non-covalent interactions are involved. In addition to that, it includes Grimme's D2 dispersion model, which additionally improves its performance to predict non-covalent interactions. These interactions play important role in envisaging the correct structure of the molecules having several electronegative elements such as LC and dye involved in this work. A more accurate description of the structures and energies can be obtained by using a double-hybrid functional APFD, which is a nine-parameter functional that uses spherical atomic model to calculate dispersion interaction. Therefore, it avoids artificial long-range attractive forces that are present in other DFT functionals due to their design. An APFD can calculate the bond length as accurately as the CCSD(T)/aug-cc-PVTZ level of theory, which is very close to the experiments [72]. Basis set 6-311++G(d,p) is adequate for elements up to the third row of the periodic table. Also, due to a lack of computational facility, we cannot test a basis set larger than set 6-311++G(d,p), but together, these two theory levels are sufficient to provides near experimental accuracy [73,74]. To build the structure of the dye-LC complex, we arranged the LC and Dye structure in such a way that rings in LC and dye stack on top of each other. The input structure of the dye-LC complex is shown in Supplementary Information Figure S1. In such a structure, we aim to simulate the $\pi - \pi$ stacking interactions, and these were optimized similarly as well. After the optimization, analytical frequency calculations were performed at the same level of theory to infer the nature of optimized structure. All the structures have positive frequencies only. Thus, they represent minimum energy structures. Optimized structures are shown in Figure 1. UV-Vis spectra were calculated from the optimized structure by applying Tamm-Dancoff approximation. Polarizability and dielectric constants were calculated at the default setting using the "polar" keyword as implemented in Gaussian 16.

3. Results and Discussion

3.1. Experimental Findings

Dielectric spectroscopy was performed in order to obtain better insights into the molecular dynamics of the LC-dye composites and to yield information about the orientation of molecular dipoles present in the guest dye molecules in the host LC system. Figure 3 illustrates the dielectric spectra corresponding to homogeneously aligned (HA) and vertically aligned (VA) dyed-LC cells as a function of frequency. Figure 3a,c show the variation in perpendicular and parallel components of dielectric permittivity (ϵ'_{\perp} and ϵ'_{\parallel}), respectively, as a function of frequency for the pure and dye-dispersed D5AOB systems. The figures express three distinct features: (i) the amount of permittivity and dielectric loss have both increased with an increasing concentration of dye in the system for HA as well as VA cells with a greater upsurge for VA cells as compared to HA ones; (ii) the dielectric anisotropy has increased significantly by 4.7-fold from 0.23 (for pristine nematic LC cell) to 1.10 (for optimum concentration, i.e., 3.0 wt% dye); and (iii) a shift in the relaxation frequency has taken place towards the longer-frequency edge from 0.70 MHz to 1.10 MHz for the parallel

component. Also, the average permittivity $\epsilon = \frac{(\epsilon'_{\parallel} + 2\epsilon'_{\perp})}{3}$ intensifies with the rise in dye concentration in the composites, as can be seen in Figure 3e. The enhancement of average permittivity points towards augmentation of capacitance of these systems, as illustrated in Figure 3f.

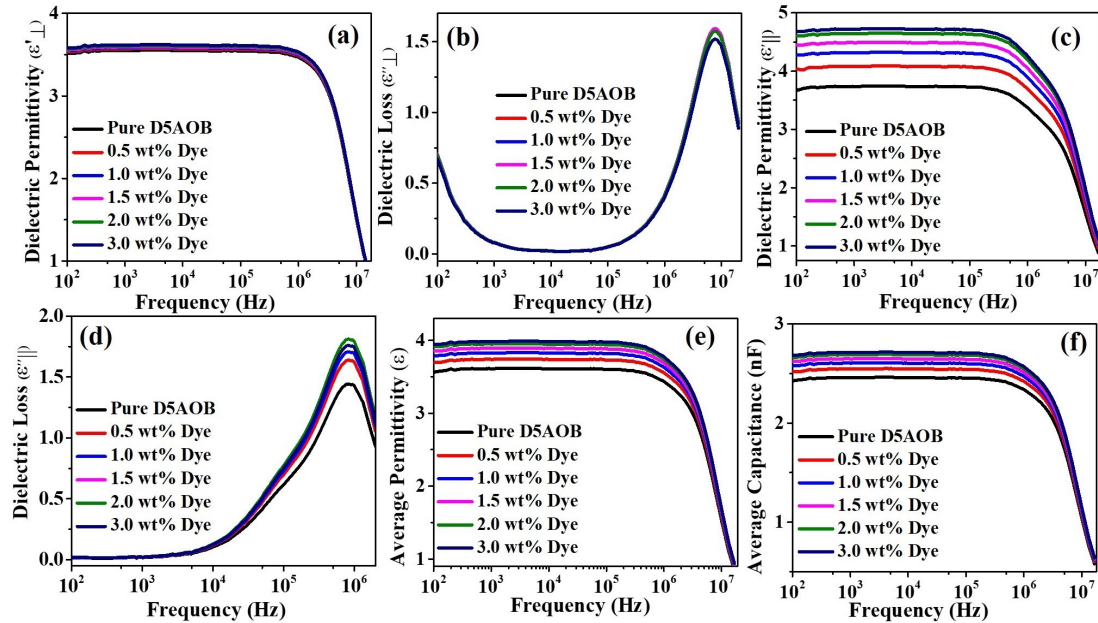


Figure 3. Dielectric spectra as a function of frequency illustrating (a) dielectric permittivity (ϵ'_{\perp}), (b) dielectric loss (ϵ''_{\perp}) for homogeneously aligned dyed-LC system, (c) dielectric permittivity (ϵ'_{\parallel}), (d) dielectric loss (ϵ''_{\parallel}) for homeotropically aligned dyed-LC system, (e) average permittivity (ϵ) and (f) average capacitance for pure NLC and composite systems.

The increment in ϵ' and $\Delta\epsilon$ points towards an additional dipolar contribution resulting from the presence of dye molecules into the weakly polar NLC matrix. The anthraquinone dye molecules, when added in the LC system, enhance the molecular ordering by aligning the dipoles and thereby tend to provide an increment in permittivity. Here, the TDM of guest 26B3OH molecules tends to align parallel to the direction of director of host molecules and hence provides a significant contribution to the dipole moment of host molecules which, in turn, modifies the collective behavior of composite systems.

The capacitance of the composite systems (C_P) estimates the ability of these materials to store electronic charges. Thus, it becomes a vital parameter for the determination of the extent of utility of a composite system in energy storage devices. It is related to dielectric permittivity (ϵ'), which is a deciding factor for probing the storage capabilities of any system, as shown by the equation

$$C_P = \frac{A\epsilon_0\epsilon'}{d} \tag{1}$$

where A is the active area of the cell ($A = 0.0004 \text{ m}^2$), and d is the cell thickness ($d = 5.2 \times 10^{-6} \text{ m}$). The variation in the average capacitance for pure and dye-dispersed LC system has been illustrated in Figure 3f, which is observed to be exhibiting an increasing trend with an increasing dye concentration.

To further explore this behavior, we examined the variation in dielectric properties of pure and dye-added composites at 20 V. The corresponding spectra are presented in Figure 4a,b, while Figure 4c,d show the trend of capacitance variation at 0 V and 20 V, respectively, with varying concentrations of dye in the composites. As expected, the increment in permittivity as well as capacitance is quite noticeable, and the results are summarized in Table 1.

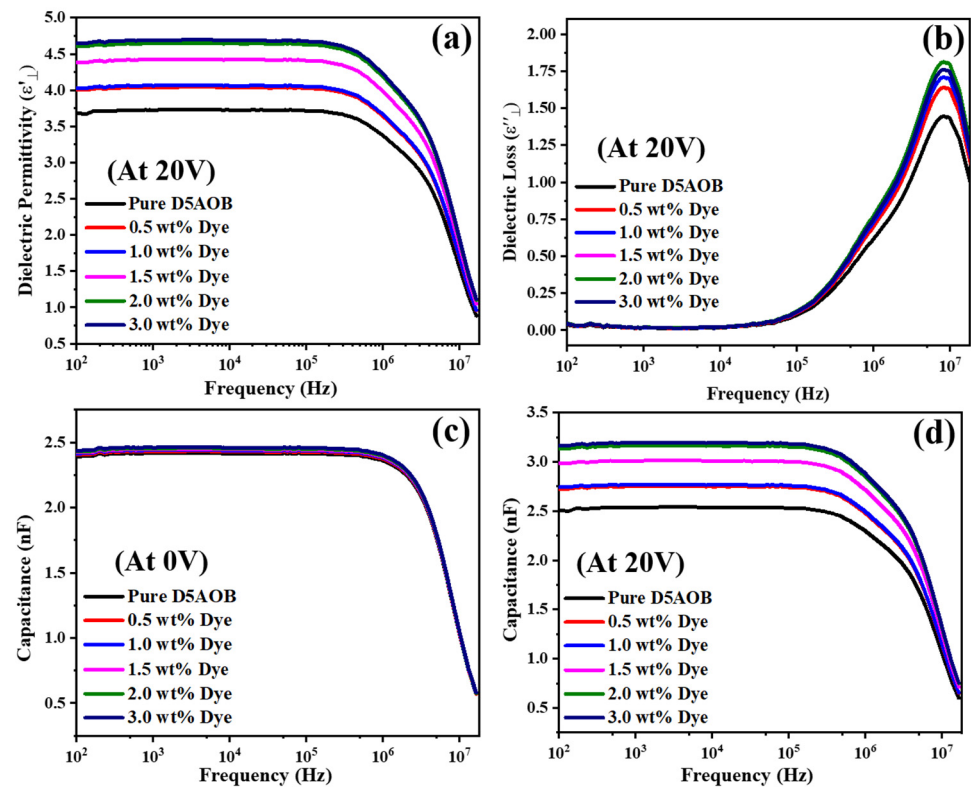


Figure 4. (a) Dielectric permittivity and (b) dielectric loss for homogeneously aligned LC cells at 20 V; capacitance of LC device as a function of frequency for pure and dye-blended systems (c) at 0 V and (d) at 20 V.

Table 1. Values of capacitance of planar-aligned LC cell for pure D5AOB and dye-dispersed D5AOB systems at 0 V and 20 V, at 1 kHz frequency of applied AC field.

Concentration of Dye	Capacitance of LC Cell (in nF)	
	At 0 V	At 20 V
Pure D5AOB	2.41	2.54
0.5 wt% Dye + D5AOB	2.42	2.75
1.0 wt% Dye + D5AOB	2.43	2.77
1.5 wt% Dye + D5AOB	2.44	3.01
2.0 wt% Dye + D5AOB	2.45	3.16
3.0 wt% Dye + D5AOB	2.46	3.19

From Table 1, it is clearly seen that the addition of dye molecules into the weakly polar nematic LC system provides an additional molecular dipole to the system, thereby enhancing its capability to store electronic charges and henceforth making it a suitable choice for energy storage applications.

Furthermore, the tunability factor [75] for dielectric spectra has also been measured at 1 kHz for pristine D5AOB and dye-dispersed systems and is defined in Equation (2) as

$$\tau = \frac{\epsilon_{\parallel} - \epsilon_{\perp}}{\epsilon_{\parallel}} \quad (2)$$

where ϵ_{\parallel} and ϵ_{\perp} measure the dielectric permittivity for VA and HA cell, respectively. It has been observed to be fostered significantly from 0.061 for pure nematic LC to 0.127, 0.169, 0.198, 0.264 and 0.293 for 0.5 wt%, 1.0 wt%, 1.5 wt%, 2.0 wt% and 3.0 wt% concentrations of dye in the host nematic LC. This high value of tunability of capacitance of LC media containing optimum concentration of dye molecules indicates its potential application not

only in energy storage devices but also as tunable media and beam steering devices. Also, the high value of the tunability factor approaching the desired mark of 0.30 opens new doors of practicality for the designed guest–host combination in 5G technologies [75]. Though we acknowledge that some other experimental validations are needed to confirm the effectiveness of this material for 5G technologies and shed more light on the mechanisms involved, it is subjected to measurements of the desired frequency range of tunability along with details about its driving voltage with suitable antenna designs, which will be performed in the future [76,77].

Furthermore, the alterations in the permittivity of system for homogenous and homeotropic alignments depicted in Figure 3 indicate a substantial enhancement of dielectric anisotropy ($\Delta\epsilon$), which points towards a noteworthy decrement of the threshold voltage (V_{th}) of pristine D5AOB system provided that the two quantities are related in accordance with the relation [5,78] given in Equation (3),

$$V_{th} = \pi \sqrt{\frac{K_{11}}{\epsilon_0 \cdot \Delta\epsilon}} \quad (3)$$

where K_{11} is the splay elastic constant and ϵ_0 is permittivity of free space.

The capacitance of a system describes its capability of storing the charges. It has been observed that the addition of dye increases the effective capacitance of the nematic system. Figure 5a depicts that the capacitance of the nematic dye composite increases with an increasing dye concentration in the host D5AOB NLC. To ensure this, V-T curves of dye-blended LC cells were measured at room temperature (RT) and are depicted in Figure 5b, which shows the decrement in threshold and operating voltage of the LC cells as apparent from the shifting of curve towards a lower-voltage edge under the influence of an increasing concentration of the dye in the system. The determination of the threshold voltage was performed using different techniques already discussed in our previously published articles [79,80], and a remarkable reduction of around 11% has been observed in them from 2.75 V for pristine D5AOB cell to 2.45 V for that containing the optimum concentration (3.0 wt%) of dye. The changes in threshold voltage and dielectric anisotropy with concentration of dye into the composites are shown in Figure 5c. This lowering of the threshold voltage and a substantial enhancement in the dielectric anisotropy ($\Delta\epsilon$) also direct towards a decrement in K_{11} .

The response time is a critical parameter for tunable LC components as it determines the performance of these materials with applied field. The rise time (fall time) is defined as the time duration required for any LC cell to change its transmission from 10% to 90% (90% to 10%) of its maximum transmission when it is turned on from 2 V to 10 V (turned off from 10 V to 2 V) and is a decisive parameter for governing how fast any LC material can respond to applied field. The turning-on process of such materials encompasses electric torque-driven reorientation of dipoles under the influence of the applied field, whereas the turning-off process involves their free relaxation reorientation. This tends to keep the rise time significantly smaller than the fall time. The variation in the rise time and fall time of dye-blended NLC cells with an elevating concentration of dyes into the system has been illustrated in Figure 5d. Notably, a 56.5% faster fall time and a 29.8% faster rise time were exhibited by the 3.0 wt% dye-doped LC cell. A lower turn-on voltage is required by the system with increasing concentrations of dye owing to the reduction in its threshold voltage and the molecular dipoles tending to reorient faster, as depicted by the decreasing rise time and fall time of the systems. The relationship of the rise time (τ_{on}) and fall time (τ_{off}) with the applied voltage (V_a) and threshold voltage (V_{th}) can be expressed [81] as seen in Equations (4) and (5):

$$\tau_{on} = \frac{\gamma d^2}{K_{11} \pi^2 \cdot \left| \left(\frac{V_a}{V_{th}} \right)^2 - 1 \right|} \quad (4)$$

$$\tau_{off} = \frac{\gamma d^2}{K_{11} \pi^2 \left| \left(\frac{V_{bias}}{V_{th}} \right)^2 - 1 \right|} \quad (5)$$

Here, K_{11} signifies the splay elastic constant, V_{bias} is the bias voltage and d denotes the thickness of LC cell. The presence of phenyl groups in the anthraquinone dye is capable of reducing the viscosity of the system and therefore contributes to reducing the response time of these composite materials. Apart from this, the cause of a large decrement in fall time in comparison to rise time can be understood as follows: Each dye molecule behaves as a dipole which tends to align with the director of the host nematic LC. However, the direction of the resultant dipole moment surrounding the local regions of the anthraquinone dye could be different from the LC director as the alignment does not occur perfectly. In the absence of an external electric field, the LC molecules near these local regions of dye molecules orient along the resultant dipole moment direction, but those far away from these regions align parallel to the glass substrates under the effect of the anchoring energy of surface. Consequently, a slight alignment imperfection could be observed in the LC matrix. On the application of sufficiently high electric field, the LC molecules in the cell tend to reorient themselves in the direction of the applied field, irrespective of their position from the local regions. Now, if the field is again switched off, the intrinsic polarization field of the dye molecules reorients the LC molecules in local regions to their previously preferred dipole moment direction, creating an additional restoring force in the system which increases with increasing concentration of the dye and hence decreases the fall time of the LC cells more rapidly.

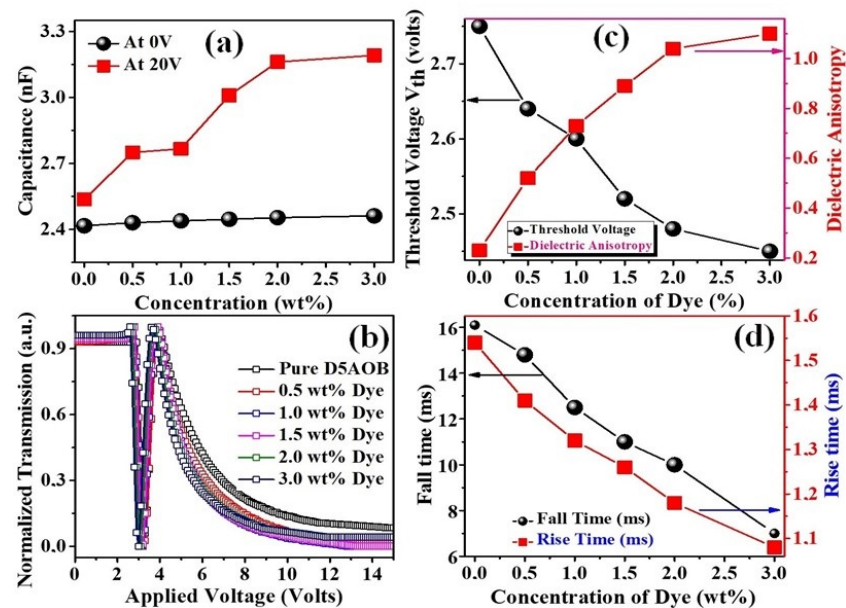


Figure 5. (a) Variation in capacitance as a function of dye concentration in the composites, for HA LC cell at 0 V and 10 V; (b) V-T curve for pure and dye-blended NLC cells; (c) variation in threshold voltage (V_{th}) and dielectric anisotropy ($\Delta\epsilon$) with concentration of dye; (d) decrement of rise time and fall time with increasing dye concentration in the LC–dye composites.

3.2. Computational Validations

In order to validate the calculated structures, we compared the UV-Vis spectra of all three structures, namely the LC, dye and LC–dye complex, calculated by us to the experimentally measured one. The results are shown in Figures S2–S4 in the Supplementary Information. The calculated UV spectra shows excellent agreement with the experimental one especially at the APFD/6-311++G(d,p) level of theory. However, it should be noted that no significant structural difference was observed when structures were calculated with wB97XD/6-

311++G(d,p) and APFD/6-311++G(d,p) level of theories. Several optical parameters like molecular polarizability (α), polarizability anisotropy ($\Delta\alpha$) and dipole moment (μ) were obtained with the help of DFT by using Equations (6) and (7) given below:

$$\alpha = \frac{\alpha_{xx} + \alpha_{yy} + \alpha_{zz}}{3} \quad (6)$$

$$\Delta\alpha = \alpha_{xx} - \frac{\alpha_{xx} + \alpha_{yy}}{2} \quad (7)$$

and

$$\beta = \sqrt{\beta_x^2 + \beta_y^2 + \beta_z^2} \quad (8)$$

Here, α_{xx} describes the molecular polarizability parallel to the long molecular axis, whereas α_{yy} and α_{zz} signify the molecular polarizabilities perpendicular to the long molecular axis. The terms β_x , β_y and β_z signify the vector components of hyperpolarizability along the x , y and z -axis, respectively. These theoretically calculated values are tabulated below in Table 2.

Table 2. Dipole moment, polarizability, polarizability anisotropy and first hyperpolarizability for D5AOB and anthraquinone dye (26B3OH) molecules calculated from optimized structures at wB97XD/6-311++G(d,p) and APFD/6-311++G(d,p) level of theory.

Molecular Systems	Dipole Moment (μ) (Multiple of 10^{-18} debye)		Polarizability (α) (Multiple of 10^{-24} esu.)		Polarizability Anisotropy ($\Delta\alpha$) (Multiple of 10^{-24} esu.)		Hyperpolarizability (β) (Multiple of 10^{-30} esu.)	
	wB97XD	APFD	wB97XD	APFD	wB97XD	APFD	wB97XD	APFD
Pure D5AOB	2.050	2.045	48.809	48.055	32.026	32.353	18.421	16.855
Pure 26B3OH	0.281	0.221	64.839	69.660	3.393	11.028	3.770	3.520
D5AOB + 26B3OH	1.874	1.576	106.729	106.729	29.626	42.733	31.672	28.927

The calculated result for the optical parameters shows no significant improvement between the two functionals. Thus, the less computationally expensive wB97XD can be used to for the investigation of the optical properties of liquid crystals. Quantum chemical calculations owe much value to the charge distribution of the molecules due to the fact that dipole moment, polarizability and many other parameters are correlated with the atomic charge strongly. The statistics about three-dimensional charge distributions and its net electrostatic effect on a molecule can be yielded and represented by a molecular electrostatic potential (MESP) diagram of the systems. It maps electrostatic potentials onto the constant electron density surface. It predicts how interactions occur between the molecules, helps in the analysis of the nature of bonding between them and assesses the reactivity of molecules towards positively or negatively charged reactants. The MESP maps for the pure D5AOB molecule, pure anthraquinone dye (26B3OH) molecule and that for D5AOB + 26B3OH are illustrated in Figure 6a–c, respectively, where the respective color schemes from deepest red to deepest blue are also shown.

MESPs also represent the electronic density sites for electrophilic and nucleophilic reactions, and the extent of the red or blue color measures the electronegativity differences as the red color appears in the regions of electrophilic reactivity, whereas blue color appears in the regions of nucleophilic reactivity with green color for neutral regions. This extensively depends upon the dipole moments, chemical reactivity, partial charges and others; therefore, total electric dipole moment (μ) was determined. Table 2 testifies that the magnitudes of total atomic dipole moment (μ), polarizability (α) and polarizability anisotropy ($\Delta\alpha$) were the largest for D5AOB + 26B3OH system, which further affirms that this system possesses strong linear optical properties. This supports the fact that the anthraquinone dye doping has increased the permittivity and dielectric anisotropy ($\Delta\epsilon$) of LC mixture significantly, as represented in Figure 3 and as discussed in section A, and the better alignment of the TDM of the 26B3OH dye molecules with the axis of molecular alignment of liquid crystal, often

described as the minimum moment of inertia (MOI) axis, can be attributed to it, which is presented in Figure 7. However, the hyperpolarizability (β) of D5AOB decreases by 7% in the D5AOB + 26B3OH system when the dye interacts with the NLC, thus limiting the non-linear optical behavior of the D5AOB + 26B3OH system. This behavior, however, needed to be tested further as CPHF, as a two-state model, is used to calculate the hyperpolarizability (β), which gives only 80% of accuracy [82].

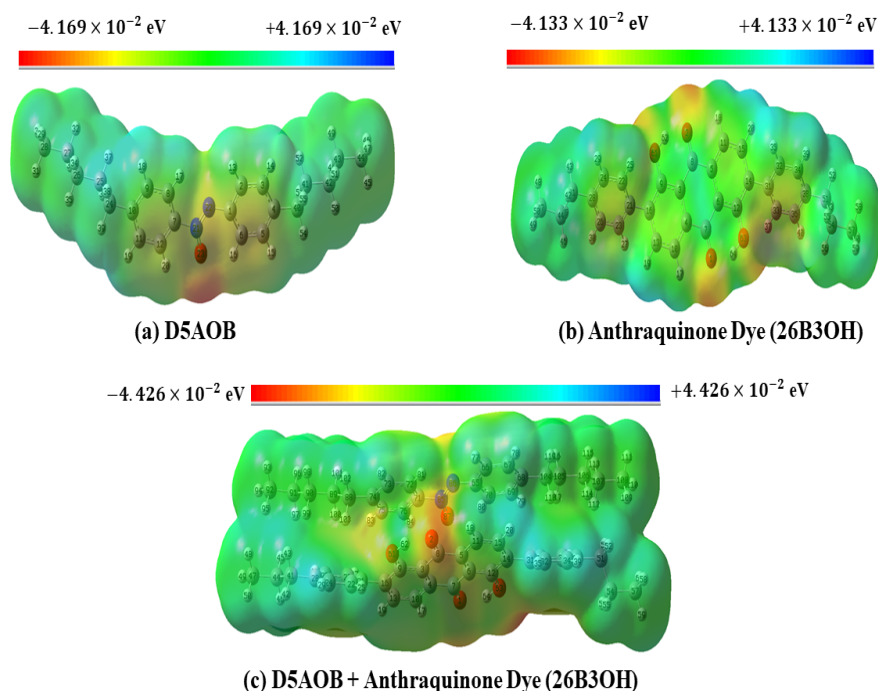


Figure 6. Molecular electrostatic potential (MESP) of (a) pure D5AOB, (b) 26B3OH dye and (c) D5AOB + 26B3OH. They are reported at APFD/6-311++G(d,p) level of theory.

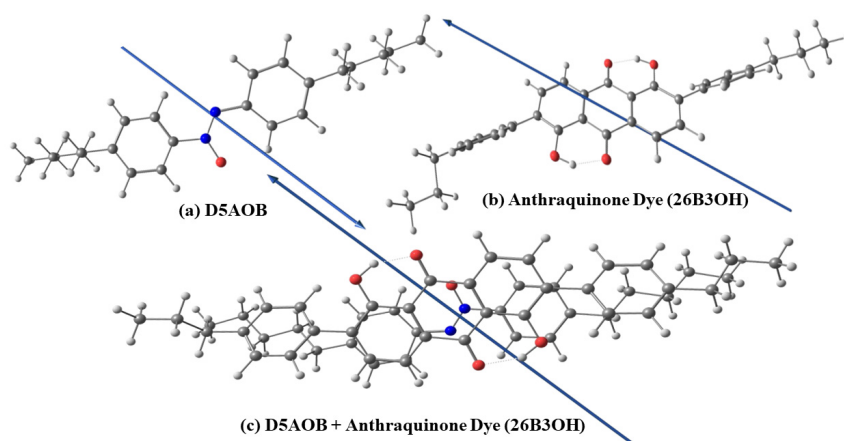


Figure 7. Orientations of TDMs (dark blue arrow) with respect to MOI axes in the optimized structures of (a) pure D5AOB, (b) pure 26B3OH dye and (c) D5AOB + 26B3OH dye.

The molecular orbital transitions between HOMO and LUMO are presented in Figures 8–10. The energy gaps (ΔE) between the HOMO and LUMO of D5AOB and 26B3OH molecules were calculated using DFT with the wB97XD/6-311++G(d,p) and APFD/6-311++G(d,p) level of theory. The energy gap is considerably answerable for the charge transfer, chemical reactivity and thermodynamic stability of molecules [83]. The different quantum chemical parameters [84] used to describe the chemical reactivity of the systems, such as chemical hardness η , softness S , electronegativity χ , electronic chemical

potential μ and index of electrophilicity ω , have been calculated using the relations given in Equations (9)–(13) and tabulated in Table 3:

$$\chi = -\frac{1}{2}(E_{LUMO} + E_{HOMO}) \tag{9}$$

$$\mu = -\chi = \frac{1}{2}(E_{LUMO} + E_{HOMO}) \tag{10}$$

$$\eta = \frac{1}{2}(E_{LUMO} - E_{HOMO}) \tag{11}$$

$$S = \frac{1}{2\eta} \tag{12}$$

$$\omega = \frac{\mu^2}{2\eta} \tag{13}$$

Table 3. Calculated values of different quantum chemical reactivity descriptors, viz. E_{HOMO} , E_{LUMO} , ΔE , χ , μ , η , S and ω for pure D5AOB, 26B3OH and D5AOB +26B3OH calculated at wB97XD/6-311++G(d,p) and APFD/6-311++G(d,p) level of theory.

Quantum Chemical Descriptors (in eV)	Pure D5AOB		Pure 26B3OH		D5AOB + 26B3OH	
	wB97XD	APFD	wB97XD	APFD	wB97XD	APFD
E_{HOMO}	−7.942	−6.227	−8.186	−6.443	−7.878	−6.165
E_{LUMO}	−0.653	−2.213	−1.642	−3.311	−1.452	−3.091
Energy Gap ΔE	7.289	4.014	6.543	3.133	6.425	3.074
χ	4.297	4.220	4.914	4.877	4.665	4.628
μ	−4.297	−4.220	−4.914	−4.877	−4.665	−4.628
η	3.645	2.007	3.272	1.566	3.213	1.537
S	0.137	0.249	0.153	0.319	0.156	0.325
ω	2.533	4.437	3.690	7.592	3.387	6.967

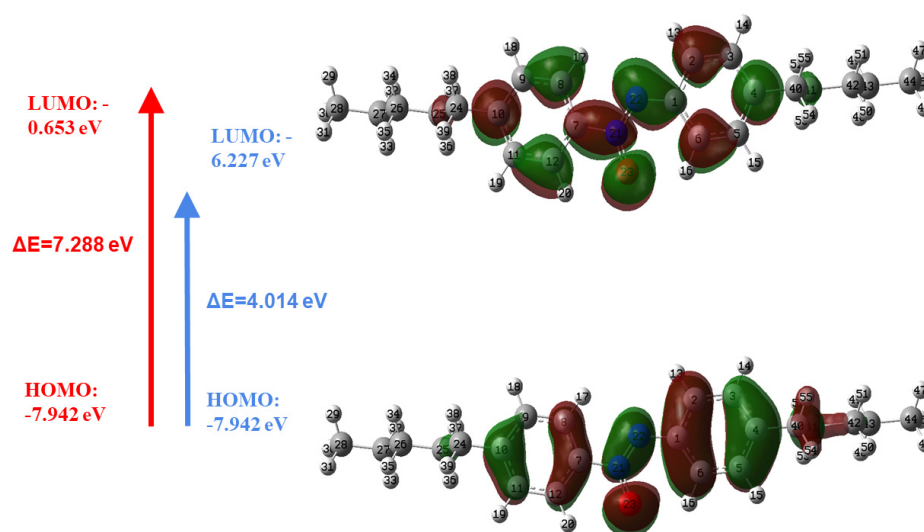


Figure 8. HOMO and LUMO for pure D5AOB nematic LC at wB97XD/6-311++G(d,p) (red arrow) and APFD/6-311++G(d,p) (blue arrow) level of theory.

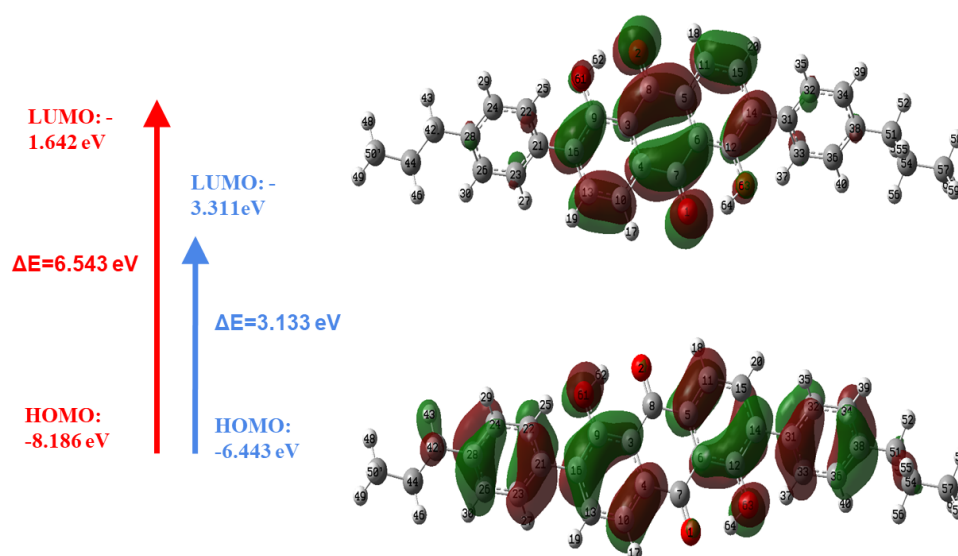


Figure 9. HOMO and LUMO for pure anthraquinone dye calculated at wB97XD/6-311++G(d,p) (red arrow) and APFD/6-311++G(d,p) (blue arrow) level of theory.

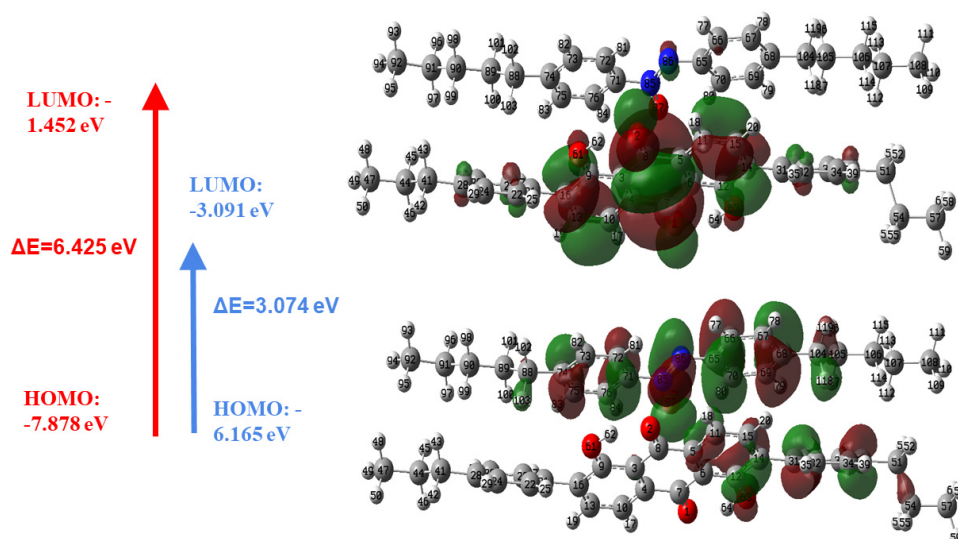


Figure 10. HOMO and LUMO for D5AOB + anthraquinone dye calculated at wB97XD/6-311++G(d,p) (red arrow) and APFD/6-311++G(d,p) (blue arrow) level of theory.

As is apparent from Table 3, we observe that the isolated dye molecule possesses the highest HOMO energy, whereas the isolated NLC molecule possesses the lowest LUMO energy. This high energy of dye molecules allows it to be the best electron donor, whereas the low energy of the NLC makes it a suitable electron acceptor. Furthermore, the NLC–dye composite system exhibits the lowest energy gap ΔE with the smallest value of hardness and greatest value of softness. It favors the system in being the softest molecule with more polarizability, high chemical reactivity and low kinetic stability. However, these quantum calculations deal with molecules in vacuum, whereas the real-time experimental conditions involve the studies in a liquid crystalline environment. Under these circumstances, molecular reorientation occurs followed by localization of electric charges that provides a sufficient amount of polarization energy to the system stabilizing ionic species in it. In effect, the HOMO and LUMO energy levels become substantially shallower and deeper, respectively [9].

As evident from figures, the computed energy gap obtained for LC–dye composite was much smaller than that for individual LC and dye molecules. A low value of ΔE causes

a highly polarized electronic structure and therefore tends to increase the dielectric constant and permittivity of the system. This is ensured by considering the values of ϵ_{\parallel} provided in Table 1. Also, the dependence of the dielectric constant $\epsilon(q)$ on the energy gap (ΔE) can be given as [85]

$$\epsilon(q) = 1 + \frac{1}{V} \frac{16\pi}{q^2} \sum_i \sum_a \frac{|\langle \varphi_i(r) | \exp(iq \cdot r) | \varphi_a(r) \rangle|^2}{E_i - E_a} \quad (14)$$

Here, ϵ is the dielectric constant, q signifies the wave vector, the indices i and a denote the occupied and unoccupied orbitals, respectively, with E_i and E_a representing the corresponding orbital energies of φ_i and φ_a states, and V is the volume of target molecule. In our case, the difference $E_i - E_a = \Delta E$ is found to be decreasing. This provides a theoretical validation to the experimentally found increment of the dielectric constant ϵ and permittivity (ϵ_{\parallel}).

4. Conclusions

In this study, we investigated the dielectric and electro-optic properties of an organic anthraquinone dye (26B3OH) dispersed within a weakly polar nematic liquid crystal (D5AOB). The major findings of this study are a manifold increment (almost 4.7 times) in the dielectric anisotropy of the weakly polar NLC on the inclusion of anthraquinone dye (26B3OH). This effective increment in the permittivity of the system also indicates towards a substantial enhancement of its charge storage capabilities. Furthermore, a reduction in the threshold voltage up to 11% was observed from the recorded V-T curves. The dyed-LC system was found to be exhibiting a 55% faster response time for the concentration of dye to be optimized at 3 wt%. This enhancement can be attributed to the additional restoring force generated by the intrinsic polarization field originating from the 26B3OH dye molecules. Additionally, the quantum chemical calculations indicated that the dispersion of the anthraquinone dye led to an increased polarizability, dipole moment and polarizability anisotropy ($\Delta\epsilon$) within the mixture. These enhancements, in turn, contributed to elevated permittivity and dielectric anisotropy in the system, aligning with our experimental findings. In conclusion, this study underscores the potential of an optimal combination of weakly polar nematic LC and organic dye for applications in energy harvesting and emerging 5G technologies due to their wide tunability range. However, it is imperative to emphasize that further in-depth research is required to fully harness the practical potential of this system for such applications.

Supplementary Materials: The following supporting information can be downloaded at: <https://www.mdpi.com/article/10.3390/jcs7110470/s1>, Figure S1: Initial structure of the dye-NLC complex used in the DFT calculations; Figure S2: A comparison between the UV-Vis spectra of pure D5AOB liquid crystal obtained experimentally and those calculated at different levels of theory. To facilitate comparison, all three spectra have been normalized. Notably, a 20 nm shift is observed between the experimental and wB97XD/6-311++G(d,p) calculated spectra. However, this shift decreases to 2 nm in the spectra calculated using the APFD/6-311++G(d,p) level of theory, which falls within an acceptable range; Figure S3: A comparison of UV-Vis spectra for the anthraquinone dye (26B3OH), showcasing both experimental and calculated spectra. All three spectra have been normalized for ease of comparison. Notably, there is an approximately 76 nm shift between the experimental spectra and those calculated at the wB97XD/6-311++G(d,p) level of theory. However, when employing the APFD/6-311++G(d,p) level of theory, this shift decreases to just 1 nm, well within an acceptable range; Figure S4: Comparison of experimental and calculated UV-Vis spectra for D5AOB + 26B3OH complex. All three spectra are normalized to unity for comparison purposes. A shift of about 24 nm from the main peak and 20 nm from the shoulder peak from experimental spectra can be seen in the spectra calculated at wB97XD/6-311++G(d,p) APFD/6-311++G(d,p) level of theory. In the case of the Dye-LC complex, both calculated spectra are identical thus they are overlapping in the above figure.

Author Contributions: Conceptualization, execution of original experiment, original draft preparation, B.P.S.; acquisition of data, reviewing and editing, S.A.; investigation, methodology, M.R.H.; DFT simulation, K.K.S.; formal analysis and validation, K.D.K.; resources and supervision, R.M.; supervision, dielectric spectroscopy, P.K.T.; reviewing and supervision of all works in France, D.P.S. All authors have read and agreed to the published version of the manuscript.

Funding: The authors are grateful to the Researchers Supporting Project number (RSP2023R222), King Saud University, Riyadh, Saudi Arabia, for the financial support. Author B.P.S. is thankful to the Department of Science and Technology (DST), New Delhi [File No. DST/INSPIRE Fellowship/2016/IF160572] for providing financial assistance in the form of an INSPIRE Fellowship. P.K.T. is grateful to Council of Science and Technology, Uttar Pradesh (CST-UP) for financial support. D.P.S. is thankful to ULCO and Pole MTE for funding.

Data Availability Statement: The data presented in this study are available on request from the corresponding authors.

Acknowledgments: The authors are grateful to the Researchers Supporting Project number (RSP2023R222), King Saud University, Riyadh, Saudi Arabia, for the financial support. Author B.P.S. is thankful to the Department of Science and Technology (DST), New Delhi [File No. DST/INSPIRE Fellowship/2016/IF160572] for providing financial assistance in the form of an INSPIRE Fellowship. P.K.T. is grateful to Council of Science and Technology, Uttar Pradesh (CST-UP) for financial support. D.P.S. is thankful to ULCO and Pole MTE for funding.

Conflicts of Interest: The authors declare no conflict of interest.

References

1. Heilmeyer, G.H.; Zanoni, L.A. Guest-host interactions in nematic liquid crystals. A new electro-optic effect. *Appl. Phys. Lett.* **2003**, *13*, 91–92. [[CrossRef](#)]
2. White, D.L.; Taylor, G.N. New absorptive mode reflective liquid-crystal display device. *J. Appl. Phys.* **2003**, *45*, 4718–4723. [[CrossRef](#)]
3. Uchida, T.; Wada, M. Guest-Host Type Liquid Crystal Displays. *Mol. Cryst. Liq. Cryst.* **1981**, *63*, 19–43. [[CrossRef](#)]
4. Seki, H.; Shishido, C.; Yasui, S.; Uchida, T. Dichroic azo dyes for guest-host liquid-crystal cell. *Jpn. J. Appl. Phys.* **1982**, *21*, 191. [[CrossRef](#)]
5. Bahadur, B. *Liquid Crystals: Applications and Uses*; World Scientific: Singapore, 1990; Volume 1.
6. Chang, I.Y.; Miller, I.K. Photostability of Anthraquinone and Azo Dyes in N-Ethylacetamide (Nylon Model). *J. Soc. Dye. Colour.* **1986**, *102*, 46–53. [[CrossRef](#)]
7. Pellatt, M.G.; Roe, I.H.C.; Constant, J. Photostable Anthraquinone Pleochroic Dyes. *Mol. Cryst. Liq. Cryst.* **1980**, *59*, 299–316. [[CrossRef](#)]
8. Iwanaga, H.; Naito, K.; Nakai, Y. The molecular structures and properties of anthraquinone-type dichroic dyes. *Mol. Cryst. Liq. Cryst. Sci. Technol. Sect. A Mol. Cryst. Liq. Cryst.* **2001**, *364*, 211–218. [[CrossRef](#)]
9. Iwanaga, H. Development of Highly Soluble Anthraquinone Dichroic Dyes and Their Application to Three-Layer Guest-Host Liquid Crystal Displays. *Materials* **2009**, *2*, 1636–1661. [[CrossRef](#)]
10. Bahadur, B. *Handbook of Liquid Crystals*; Demus, D., Goodby, J., Gray, G.W., Spiess, H.W., Vill, V., Eds.; Low Molecular Weight Liquid Crystals; John Wiley & Sons: Hoboken, NJ, USA, 1998; Volume 2, pp. 296–297.
11. Saunders, F.; Harrison, K.; Raynes, E.; Thompson, D. New photostable anthraquinone dyes with high order parameters. *IEEE Trans. Electron Devices* **1983**, *30*, 499–503. [[CrossRef](#)]
12. Pelzl, G.; Zschke, H.; Demus, D. Liquid crystalline tetrazine compounds as dyes for guest-host displays with positive contrast. *Displays* **1985**, *6*, 141–147. [[CrossRef](#)]
13. Wolarz, E.; Moryson, H.; Bauman, D. Dichroic fluorescent dyes for ‘guest-host’ liquid crystal displays. *Displays* **1992**, *13*, 171–178. [[CrossRef](#)]
14. Bauman, D.; Mykowska, E.; Wolarz, E. Molecular orientation of perylene-like dyes in liquid crystal 80CB. *Mol. Cryst. Liq. Cryst. Sci. Technol. Sect. A Mol. Cryst. Liq. Cryst.* **1998**, *321*, 333–347. [[CrossRef](#)]
15. Chen, Z.; Swager, T.M. Synthesis and characterization of fluorescent acenequinones as dyes for guest-host liquid crystal displays. *Org. Lett.* **2007**, *9*, 997–1000. [[CrossRef](#)] [[PubMed](#)]
16. Sim, Y.; Choi, H. Creation of topological charges by the spontaneous symmetry breaking phase transition in azo dye-doped nematic liquid crystals. *Opt. Mater. Express* **2022**, *12*, 174–183. [[CrossRef](#)]
17. Ji, W.; Wang, Z.; Huang, N.; Liu, H. Reconstruction of weak near-infrared images in methyl red-doped nematic liquid crystals via stochastic resonance. *Opt. Express* **2022**, *30*, 30108–30120. [[CrossRef](#)] [[PubMed](#)]
18. Lesiuk, A.; Ledney, M.; Reshetnyak, V.Y. Light-induced Fredericks transition in the nematic liquid crystal cell with plasmonic nanoparticles at a cell bounding substrate. *Phys. Rev. E* **2022**, *106*, 024706. [[CrossRef](#)]

19. Gollapelli, B.; Rama Raju Ganji, S.; Kumar Tatipamula, A.; Vallamkondu, J. Bio-derived chlorophyll dye doped cholesteric liquid crystal films and microdroplets for advanced anti-counterfeiting security labels. *J. Mol. Liq.* **2022**, *363*, 119952. [CrossRef]
20. Huang, Y.-M.; Chang, L.-M.; Wang, C.-T. Electrically induced bistable switching of stop band in chiral nematic photonic crystal. *J. Mol. Liq.* **2022**, *365*, 120133. [CrossRef]
21. Funahashi, M. High open-circuit voltage under the bulk photovoltaic effect for the chiral smectic crystal phase of a double chiral ferroelectric liquid crystal doped with a fullerene derivative. *Mater. Chem. Front.* **2021**, *5*, 8265–8274. [CrossRef]
22. Feng, C.; Saha, R.; Korblova, E.; Walba, D.; Sprunt, S.N.; Jáklí, A. Electrically Tunable Reflection Color of Chiral Ferroelectric Nematic Liquid Crystals. *Adv. Opt. Mater.* **2021**, *9*, 2101230. [CrossRef]
23. Zhang, X.; Wu, L.; Chen, K.; Liu, W.; Li, B.; Li, Y.; Yang, Y. Mesomorphic behaviors of some acrylate liquid crystals and their application for polarizer preparation. *Liq. Cryst.* **2022**, *49*, 418–425. [CrossRef]
24. Funahashi, M. Chiral liquid crystalline electronic systems. *Symmetry* **2021**, *13*, 672. [CrossRef]
25. Ji, W.; Shi, L.-Y.; Tang, H.; Sun, G.; Hu, W.; Liang, X. Large birefringence smectic-A liquid crystals for high contrast bistable displays. *Opt. Mater. Express* **2015**, *5*, 281–286. [CrossRef]
26. Gardiner, D.J.; Coles, H.J. Enhancing lifetime in a bistable smectic A liquid crystal device. *J. Phys. D Appl. Phys.* **2007**, *40*, 977–981. [CrossRef]
27. Fritsch, L.; Mandle, R.J.; Cowling, S.J.; Goodby, J.W. Carbosilane terminated alkoxybiphenyls for bistable scattering mode LCDs. *J. Mater. Chem. C* **2021**, *9*, 714–718. [CrossRef]
28. Sheng, M.; Zhang, L.; Jiang, S.; Yang, L.; Zaaboul, F.; Fu, S. Bioinspired Electro-Responsive Multispectral Controllable Dye-Doped Liquid Crystal Yolk–Shell Microcapsules for Advanced Textiles. *ACS Appl. Mater. Interfaces* **2021**, *13*, 13586–13595. [CrossRef]
29. Sheng, M.; Li, J.; Jiang, X.; Wang, C.; Li, J.; Zhang, L.; Fu, S. Biomimetic solid–liquid transition structural dye-doped liquid crystal/phase-change-material microcapsules designed for wearable bistable electrochromic fabric. *ACS Appl. Mater. Interfaces* **2021**, *13*, 33282–33290. [CrossRef]
30. Xiong, J.; Wu, S.-T. Planar liquid crystal polarization optics for augmented reality and virtual reality: From fundamentals to applications. *eLight* **2021**, *1*, 3. [CrossRef]
31. Zhan, T. Liquid Crystal Flat Optics for Near-Eye Displays. Ph.D. Thesis, University of Central Florida, Orlando, FL, USA, 2021; p. 591. Available online: <https://stars.library.ucf.edu/etd2020/591> (accessed on 17 September 2023).
32. Kocakulah, G.; Köysal, O.; Kahyaoglu, A. Electro-Optical performance investigation of cholesteric liquid crystal containing azo dye: Light shutter device application. *J. Electron. Mater.* **2021**, *50*, 497–510. [CrossRef]
33. Xie, X.; Huang, P.; Xu, M.; Ding, Y.; Qiu, L.; Lu, H. Tri-state switching of a high-order parameter, double-layered guest-host liquid-crystal shutter, doped with the mesogenic molecule 4HPB. *Liq. Cryst.* **2021**, *48*, 1555–1561. [CrossRef]
34. Popov, P.; Mann, E.K.; Jakli, A. Thermotropic liquid crystal films for biosensors and beyond. *J. Mater. Chem. B* **2017**, *5*, 5061–5078. [CrossRef] [PubMed]
35. Lee, M.-J.; Lee, W. Liquid crystal-based biosensing: Exploiting the electrical and optical properties of various liquid crystals in quantitative bioassays. In *Unconventional Liquid Crystals and Their Applications*; Walter de Gruyter GmbH & Co. KG: Berlin, Germany, 2021; p. 239. [CrossRef]
36. Mysliwiec, J.; Szukalska, A.; Szukalski, A.; Sznitko, L. Liquid crystal lasers: The last decade and the future. *Nanophotonics* **2021**, *10*, 2309–2346. [CrossRef]
37. Hsu, C.J.; Singh, B.P.; Selvaraj, P.; Antony, M.; Manohar, R.; Huang, C.Y. Superior improvement in dynamic response of liquid crystal lens using organic and inorganic nanocomposite. *Sci. Rep.* **2021**, *11*, 17349. [CrossRef] [PubMed]
38. Selvaraj, P.; Subramani, K.; Srinivasan, B.; Hsu, C.-J.; Huang, C.-Y. Electro-optical effects of organic N-benzyl-2-methyl-4-nitroaniline dispersion in nematic liquid crystals. *Sci. Rep.* **2020**, *10*, 14273. [CrossRef]
39. Zhu, C.; Lu, Y.; Jiang, L.; Yu, Y. Liquid crystal soft actuators and robots toward mixed reality. *Adv. Funct. Mater.* **2021**, *31*, 2009835. [CrossRef]
40. Li, Y.; Liu, Y.; Luo, D. Polarization dependent light-driven liquid crystal elastomer actuators based on photothermal effect. *Adv. Opt. Mater.* **2021**, *9*, 2001861. [CrossRef]
41. Oh, S.-W.; Ji, S.-M.; Han, C.-H.; Yoon, T.-H. A cholesteric liquid crystal smart window with a low operating voltage. *Dye. Pigment.* **2022**, *197*, 109843. [CrossRef]
42. Zhang, Y.; Yang, X.; Zhan, Y.; Zhang, Y.; He, J.; Lv, P.; Yuan, D.; Hu, X.; Liu, D.; Broer, D.J. Electroconvection in zwitterion-doped nematic liquid crystals and application as smart windows. *Adv. Opt. Mater.* **2021**, *9*, 2001465. [CrossRef]
43. Yao, K.; Li, Y.; Shen, Y.; Quan, Y.; Cheng, Y. A photosensitive-type CPL response controlled by intermolecular dynamic FRET and chiral transfer in ternary chiral emissive nematic liquid crystals. *J. Mater. Chem. C* **2021**, *9*, 12590–12595. [CrossRef]
44. Lutfor, M.R.; Hegde, G.; Kumar, S.; Tschierske, C.; Chigrinov, V.G. Synthesis and characterization of bent-shaped azobenzene monomers: Guest–host effects in liquid crystals with azo dyes for optical image storage devices. *Opt. Mater.* **2009**, *32*, 176–183. [CrossRef]
45. Wang, X.; Lu, X.; Liu, B.; Chen, D.; Tong, Y.; Shen, G. Flexible energy-storage devices: Design consideration and recent progress. *Adv. Mater.* **2014**, *26*, 4763–4782. [CrossRef] [PubMed]
46. Liu, C.; Li, F.; Ma, L.P.; Cheng, H.M. Advanced materials for energy storage. *Adv. Mater.* **2010**, *22*, E28–E62. [CrossRef] [PubMed]
47. Tyagi, A.; Tripathi, K.M.; Gupta, R.K. Recent progress in micro-scale energy storage devices and future aspects. *J. Mater. Chem. A* **2015**, *3*, 22507–22541. [CrossRef]

48. Yang, P.; Sun, P.; Mai, W. Electrochromic energy storage devices. *Mater. Today* **2016**, *19*, 394–402. [[CrossRef](#)]
49. Xia, M.; Nie, J.; Zhang, Z.; Lu, X.; Wang, Z.L. Suppressing self-discharge of supercapacitors via electrorheological effect of liquid crystals. *Nano Energy* **2018**, *47*, 43–50. [[CrossRef](#)]
50. Devaki, S.J.; Sasi, R. Ionic liquids/ionic liquid crystals for safe and sustainable energy storage systems. In *Progress and Developments in Ionic Liquids*; InTech: Rijeka, Croatia, 2017; pp. 313–336.
51. Ruan, Q.; Yao, M.; Yuan, D.; Dong, H.; Liu, J.; Yuan, X.; Fang, W.; Zhao, G.; Zhang, H. Ionic liquid crystal electrolytes: Fundamental, applications and prospects. *Nano Energy* **2022**, *106*, 108087. [[CrossRef](#)]
52. Salikolimi, K.; Sudhakar, A.A.; Ishida, Y. Functional ionic liquid crystals. *Langmuir* **2020**, *36*, 11702–11731. [[CrossRef](#)]
53. Ibrahim, A.R.; Khyasudeen, M.F.; Husband, J.; Alauddin, S.M.; Aripin, N.F.K.; Velayutham, T.S.; Martinez-Felipe, A.; Abou-Zied, O.K. p-Methoxy Azobenzene Terpolymer as a Promising Energy-Storage Liquid Crystal System. *J. Phys. Chem. C* **2021**, *125*, 22472–22482. [[CrossRef](#)]
54. Singh, D.P.; Vimal, T.; Mange, Y.J.; Varia, M.C.; Nann, T.; Pandey, K.; Manohar, R.; Douali, R. CuInS₂/ZnS QD-ferroelectric liquid crystal mixtures for faster electro-optical devices and their energy storage aspects. *J. Appl. Phys.* **2018**, *123*, 034101. [[CrossRef](#)]
55. Liu, X.; Luo, H.; Yan, C.; Liu, Y.; Luo, H.; Zhang, D.; Chen, S. Achieving synergistic improvement in dielectric constant and energy storage properties of all-organic liquid crystal molecule/PVDF composites. *J. Mater. Chem. C* **2022**, *10*, 17757–17767. [[CrossRef](#)]
56. Liu, H.; Tang, Y.; Wang, C.; Xu, Z.; Yang, C.; Huang, T.; Zhang, F.; Wu, D.; Feng, X. A Lyotropic Liquid-Crystal-Based Assembly Avenue toward Highly Oriented Vanadium Pentoxide/Graphene Films for Flexible Energy Storage. *Adv. Funct. Mater.* **2017**, *27*, 1606269. [[CrossRef](#)]
57. Xia, Y.; Mathis, T.S.; Zhao, M.-Q.; Anasori, B.; Dang, A.; Zhou, Z.; Cho, H.; Gogotsi, Y.; Yang, S. Thickness-independent capacitance of vertically aligned liquid-crystalline MXenes. *Nature* **2018**, *557*, 409–412. [[CrossRef](#)] [[PubMed](#)]
58. Wu, P.-C.; Hou, C.-T.; Hsiao, Y.-C.; Lee, W. Influence of methyl red as a dopant on the electrical properties and device performance of liquid crystals. *Opt. Express* **2014**, *22*, 31347–31355. [[CrossRef](#)] [[PubMed](#)]
59. Zhao, C.; Hu, Y.; Xu, J.; Yu, M.; Zou, C.; Wang, Q.; Gao, Y.; Yang, H. Research on the Morphology, Electro-Optical Properties and Mechanical Properties of Electrochromic Polymer-Dispersed Liquid Crystalline Films Doped with Anthraquinone Dyes. *Crystals* **2023**, *13*, 735. [[CrossRef](#)]
60. Kocakülal, G.; Köysal, O. Conductivity and optical bandgap parameters variations of methyl red-doped 4-pentyl-4'-cyanobiphenyl nematic liquid crystal: Norland optical adhesive 65 photopolymer composites. *J. Mater. Sci. Mater. Electron.* **2023**, *34*, 1498. [[CrossRef](#)]
61. Katariya-Jain, A.; Deshmukh, R.R. Effects of dye doping on electro-optical, thermo-electro-optical and dielectric properties of polymer dispersed liquid crystal films. *J. Phys. Chem. Solids* **2022**, *160*, 110363. [[CrossRef](#)]
62. Shen, W.; Zhang, H.; Miao, Z.; Ye, Z. Recent Progress in Functional Dye-Doped Liquid Crystal Devices. *Adv. Funct. Mater.* **2023**, *33*, 2210664. [[CrossRef](#)]
63. Kumar, P.; Sharma, V.; Raina, K.K. Studies on inter-dependency of electrooptic characteristics of orange azo and blue anthraquinone dichroic dye doped polymer dispersed liquid crystals. *J. Mol. Liq.* **2018**, *251*, 407–416. [[CrossRef](#)]
64. Agarwal, S.; Singh, B.P.; Tripathi, S.; Srivastava, P.; Sharma, S.; Manohar, R. Inquisitive Optical and Electro-Optical Attributes of Azo-Dye Dispersed Nematic Liquid Crystal for Applications in Wavelength-Tunable Optical Filters. *J. Phys. Chem. C* **2023**, *127*, 20466–20476. [[CrossRef](#)]
65. Oka, A.; Sinha, G.; Glorieux, C.; Thoen, J. Broadband dielectric studies of weakly polar and non-polar liquid crystals. *Liq. Cryst.* **2004**, *31*, 31–38. [[CrossRef](#)]
66. Cowling, S.J.; Ellis, C.; Goodby, J.W. Anthraquinone Liquid crystal dichroic dyes—A new form of chromonic dye? *Liq. Cryst.* **2011**, *38*, 1683–1698. [[CrossRef](#)]
67. Sims, M.T.; Abbott, L.C.; Cowling, S.J.; Goodby, J.W.; Moore, J.N. Molecular Design Parameters of Anthraquinone Dyes for Guest–Host Liquid-Crystal Applications: Experimental and Computational Studies of Spectroscopy, Structure, and Stability. *J. Phys. Chem. C* **2016**, *120*, 11151–11162. [[CrossRef](#)]
68. Singh, B.P.; Huang, C.Y.; Singh, D.P.; Palani, P.; Duponchel, B.; Sah, M.; Manohar, R.; Pandey, K.K. The scientific duo of TiO₂ nanoparticles and nematic liquid crystal E204: Increased absorbance, photoluminescence quenching and improving response time for electro-optical devices. *J. Mol. Liq.* **2021**, *325*, 115130. [[CrossRef](#)]
69. Singh, B.P.; Sikarwar, S.; Agrahari, K.; Tripathi, S.; Gangwar, R.K.; Manohar, R.; Pandey, K.K. Electro-optical characterization of a weakly polar liquid crystalline compound influenced polyvinyl pyrrolidone capped gold nanoparticles. *J. Mol. Liq.* **2021**, *325*, 115172. [[CrossRef](#)]
70. Dennington, R.; Keith, T.; Millam, J. *Shawnee Mission KS, GaussView, Version*; Semichem Inc.: Seoul, Republic of Korea, 2009; Volume 5.
71. Frisch, M.J.; Trucks, G.W.; Schlegel, H.B.; Scuseria, G.E.; Robb, M.A.; Cheeseman, J.R.; Scalmani, G.; Barone, V.; Petersson, G.A.; Nakatsuji, H.; et al. *Gaussian 16 Rev. C.01*; Gaussian Headquarters: Wallingford, CT, USA, 2016.
72. Austin, A.; Petersson, G.A.; Frisch, M.J.; Dobek, F.J.; Scalmani, G.; Throssell, K. A density functional with spherical atom dispersion terms. *J. Chem. Theory Comput.* **2012**, *8*, 4989–5007. [[CrossRef](#)]
73. Das, M.; Singh, K.K.; Khan, E.; Sinha, R.K.; Singh, R.K.; Tandon, P.; Gangopadhyay, D. N-Acetylcysteine versus arsenic poisoning: A mechanistic study of complexation by molecular spectroscopy and density functional theory. *J. Mol. Liq.* **2021**, *340*, 117168. [[CrossRef](#)]

74. Wititsuwannakul, T.; Mukherjee, T.; Hall, M.B.; Gladysz, J.A. Computational investigations of enantioselection in carbon–carbon bond forming reactions of ruthenium guanidinobenzimidazole second coordination sphere hydrogen bond donor catalysts. *Organometallics* **2020**, *39*, 1149–1162. [[CrossRef](#)]
75. Manabe, A. *Liquid Crystals for Microwave Applications*; SPIE: Bellingham, WA, USA, 2013; Volume 8642.
76. Liu, H.; Avrutin, V.; Zhu, C.; Özgür, Ü.; Yang, J.; Lu, C.; Morkoç, H. Enhanced microwave dielectric tunability of Ba_{0.5}Sr_{0.5}TiO₃ thin films grown with reduced strain on DyScO₃ substrates by three-step technique. *J. Appl. Phys.* **2013**, *113*, 044108. [[CrossRef](#)]
77. Gaebler, A.; Moessinger, A.; Goelden, F.; Manabe, A.; Goebel, M.; Follmann, R.; Koether, D.; Modes, C.; Kipka, A.; Deckelmann, M.; et al. Liquid Crystal-Reconfigurable Antenna Concepts for Space Applications at Microwave and Millimeter Waves. *Int. J. Antennas Propag.* **2009**, *2009*, 876989. [[CrossRef](#)]
78. Helfrich, W. Electric alignment of liquid crystal. *Mol. Cryst. Liq. Cryst.* **1973**, *21*, 187–209. [[CrossRef](#)]
79. Singh, B.P.; Sikarwar, S.; Pandey, K.K.; Duraisamy, S.; Gupta, S.K.; Manohar, R. Nematic Liquid Crystals Dispersed with Thermoelectric Gallium Oxide (Ga₂O₃) Microrods: A Perspective for Improving the Response Time of Electro-Optical Devices. *J. Phys. Chem. C* **2022**, *126*, 15924–15935. [[CrossRef](#)]
80. Singh, B.P.; Sikarwar, S.; Manohar, R.; Shah, A.; Singh, D.P.; Herman, J.; Pandey, K.K. Nematic liquid crystals blended ferroelectric nanoparticles (BaTiO₃): A perspective way for improving the response time and photoluminescence for electro-optical devices. *J. Appl. Phys.* **2022**, *131*, 174102. [[CrossRef](#)]
81. Schadt, M. Liquid crystal materials and liquid crystal displays. *Annu. Rev. Mater. Sci.* **1997**, *27*, 305–379. [[CrossRef](#)]
82. Kocherzhenko, A.A.; Shedge, S.V.; Sosa Vazquez, X.; Maat, J.; Wilmer, J.; Tillack, A.F.; Johnson, L.E.; Isborn, C.M. Unraveling excitonic effects for the first hyperpolarizabilities of chromophore aggregates. *J. Phys. Chem. C* **2019**, *123*, 13818–13836. [[CrossRef](#)]
83. Garg, U.; Azim, Y.; Alam, M. In acid-aminopyrimidine continuum: Experimental and computational studies of furan tetracarboxylate-2-aminopyrimidinium salt. *RSC Adv.* **2021**, *11*, 21463–21474. [[CrossRef](#)]
84. Abbaz, T.; Bendjeddou, A.; Villemin, D. Molecular structure, HOMO, LUMO, MEP, natural bond orbital analysis of benzo and anthraquinodimethane derivatives. *Pharm. Biol. Eval.* **2018**, *5*, 27. [[CrossRef](#)]
85. Shimazaki, T.; Nakajima, T. Application of the dielectric-dependent screened exchange potential approach to organic photocell materials. *Phys. Chem. Chem. Phys.* **2016**, *18*, 27554–27563. [[CrossRef](#)]

Disclaimer/Publisher’s Note: The statements, opinions and data contained in all publications are solely those of the individual author(s) and contributor(s) and not of MDPI and/or the editor(s). MDPI and/or the editor(s) disclaim responsibility for any injury to people or property resulting from any ideas, methods, instructions or products referred to in the content.